European Radiology (2019) 29:3253–3261
https://doi.org/10.1007/s00330-018-5843-y

MUSCULOSKELETAL

Accuracy of iodine density thresholds for the separation of vertebral bone metastases from healthy-appearing trabecular bone in spectral detector computed tomography

Jan Borggrefe[1] · Victor-Frederic Neuhaus[1] · Markus Le Blanc[1] · Nils Grosse Hokamp[1] · Volker Maus[1] · Anastasios Mpotsaris[1] · Simon Lennartz[1] · Daniel Pinto dos Santos[1] · David Maintz[1] · Nuran Abdullayev[1]

Received: 12 April 2018 / Revised: 14 September 2018 / Accepted: 19 October 2018 / Published online: 6 December 2018

Abstract

Purpose To evaluate quantitative iodine density mapping (IDM) with spectral detector computed tomography (SDCT) as a quantitative biomarker for separation of vertebral trabecular bone metastases (BM) from healthy-appearing trabecular bone (HTB).

Materials and methods IRB-approved retrospective single-center-study of portal venous SDCT datasets acquired between June 2016 and March 2017. Inclusion of 43 consecutive cancer patients with BM and 40 without. Target lesions and non-affected control vertebrae were defined using follow-up imaging, MRI, and/or bone scintigraphy. ID and standard deviation were determined with ROI measures by two readers in (a) bone metastases, (b) HTB of BM patients and controls, and (c) ID of various vessels. Volumetric bone mineral density (vBMD) of the lumbar spine and age were recorded. Multivariate ROC analyses und Wilcoxon test were used to determine thresholds for separation of BM and HTB. $p < 0.05$ was considered significant.

Results ID measurements of 40 target lesions and 83 reference measurements of HTB were acquired. Age ($p < 0.0001$) and vBMD ($p < 0.05$) affected ID measurements independently in multivariate models. There were significant differences of ID between metastases ($n = 43$) and HTB ID ($n = 124$; mean 5.5 ± 0.9 vs. 3.5 ± 0.9; $p < 0.0001$), however, with considerable overlap. In univariate analysis, increased ID discriminated bone lesions (AUC 0.90) with a maximum combined specificity/sensitivity of 77.5%/90.7% when applying a threshold of 4.5 mg/ml. Multivariate regression models improved significantly when considering vBMD, the noise of ID, and vertebral venous ID (AUC 0.98).

Conclusion IDM of SDCT yielded a statistical separation of vertebral bone lesions and HTB. Adjustment for confounders such as age and lumbar vBMD as well as for vertebral venous ID and lesion heterogeneity improved discrimination of trabecular lesions.

Key Points

- *SDCT iodine density mapping provides the possibility for quantitative analysis of iodine uptake in tissue, which allows to differentiate bone lesions from healthy bone marrow.*
- *Age and vBMD have a significant impact on iodine density measurements.*
- *Iodine density measured in SDCT yielded highest sensitivity and specificity for the statistical differentiation of vertebral trabecular metastases and healthy trabecular bone using an iodine density threshold of 4.5 mg/ml (most performant)–5.0 mg/ml (optimized for specificity).*

Keywords Bone · Tomography · Iodine · Diagnosis · Neoplasm metastasis

Electronic supplementary material The online version of this article (https://doi.org/10.1007/s00330-018-5843-y) contains supplementary material, which is available to authorized users.

✉ Jan Borggrefe
Jan.Borggrefe@uk-koeln.de

[1] Institut für Diagnostische und Interventionelle Radiologie, Uniklinik Köln, Kerpener Str. 62, 50935 Köln, Germany

Abbreviations

CT	Computed tomography
BMD	Bone mineral density
BM	Bone metastases
HTB	Healthy trabecular bone
ID	Iodine density
IDM	Iodine density mapping
SDCT	Spectral detector computed tomography

UICC Union for International Cancer Control
WHO World Health Organization

Introduction

Bone metastases (BM) are associated with advanced stage of cancer and poor prognosis [1–4]. Detection of these lesions is crucial to adapt individual treatment and to prevent potential skeletal complications such as fractures and severe pain [5–7].

Contrast-enhanced computed tomography (CT) is routinely acquired for staging and for follow-up of patients with a history of cancer, although CT is known to allow only for a limited detection of bone metastases [8]. Especially diffuse bone metastases are hardly detectable with CT when they are neither destroying bone nor causing osteoblastic bone changes (Table 1) [9]. Thus, additional diagnostic examinations such as 99mTc bone scan, PET-CT, or MRI are performed frequently.

Recently, spectral detector CT (SDCT) was introduced into clinical routine, a single source CT scanner with a dual-layer detector. In contrast to emission-based techniques of dual-energy CT, the dual layer detector allows for separate detection of photons according to their energy [10, 11]. Besides material decomposition, the method allows for the local volumetric quantification of iodine density (ID) [11, 12]. To date, it is unclear if ID quantification and visualization may be relevant for clinical diagnostics, e.g., for the differentiation of diffuse osseous lesions. However, in earlier studies, it has been shown that dual energy CT allows for a differentiation of malignant and benign bone lesions such as bone islands and Schmorl's nodes [13, 14]. Furthermore, monoenergetic reconstructions of SDCT are improving image quality and lesion characterization [15–17].

Tumor growth is dependent on the development of new blood vessels, a process referred to as neovascularization [18, 19]. Hence, bone metastases show a strong enhancement of tumor tissues after intravenous administration of contrast agents [20–24]. Thus, in comparison with conventional single-energy CT, it appears likely that the dedicated detection of the iodine concentration with SDCT might improve the sensitivity for the detection and differentiation of malignant vertebral lesions, especially diffuse bone marrow lesions. SDCT might enable clinicians to perform a more accurate staging of bone lesions and, in addition, could allow to improve RECIST or MDA criteria, which in regard to bone lesions are only applicable to a limited extend [25]. However, the prevalent calcium content within the bone might interfere with the detection of iodine density as both materials show similar characteristics in dual energy, thus impairing the detection of increased iodine uptake within metastases. Further, bone density as well as iodine density of normal and pathologic tissues might vary considerably in dependence of patient age which might prohibit the differentiation of regular vertebral trabecular bone and pathologic bone lesions.

In our personal clinical experience, SDCT iodine mapping detected bone lesions that were not seen on conventional CT images. Therefore, we hypothesized that iodine density measurements allow to separate bone metastases from healthy trabecular bone. In order to provide basic knowledge for future clinical studies, we investigated (a) the feasibility and performance of iodine density quantification with dual-layer computed tomography as a statistical biomarker of bone lesions and unaffected trabecular bone, (b) confounders of iodine mapping in healthy trabecular bone, and (c) iodine thresholds that could serve as cut-off values for malignant bone lesions in automated patient evaluation or every day routine image reading.

Material and methods

Study population and determination of target lesions

The presented retrospective single-center study was approved by the local ethics committee with waved informed consent

Table 1 Suitability of imaging modalities for the assessment of bone metastasis features (green box = suitable, following Heindel et al [9]). Computed tomography is a standard method for staging of cancer patients with dedicated advantages in the detection of structural bone changes. However, in comparison to MRI and positron emission tomography, CT has methodological impairments to detect diffuse bone marrow lesions and to characterize metabolic changes within the bones. Iodine density mapping of spectral detector CT may allow to improve bone marrow lesion characterization with CT (marked yellow) by allowing to detect diffuse bone lesions within the bone marrow by increasing image contrast and by allowing for iodine and edema mapping based on abilities to perform material decomposition within CT images

	Bone morphology	Bone microstructure	Marrow involvement	Bone metabolism	Glucose metabolism	Diffusion
Projectional radiography						
Conventional CT						
Spectral detector CT						
Single Photon Emission CT						
MRI						
PET-CT						
PET-MRI						

(registration number 17-257) and conducted in order to test if limitations of computed tomography in the depiction and quantification of diffuse vertebral metastases can be overcome with the use iodine mapping (Table 1, Fig. 1). Out of all our patients that received CT for cancer staging in the period between June 2016 and March 2017, we retrospectively identified all consecutive patients with lung cancer and breast cancer that showed vertebral bone metastases ($n = 43$). There were 21 cases with osteoblastic bone metastases (BBM Fig. 2) and 22 cases with osteolytic bone metastases (LBM). As a control group, we selected a random subset of 40 patients with lung and breast cancer that received CT for cancer staging in the same period without detectable bone metastases (NoBM). Inclusion criteria were (Table 2) (a) SDCT study within the provided time period, (b) diagnosis of lung cancer or breast cancer, (c) prevalence of bone metastases, and (d) verification of target lesions in either a 6-month follow-up CT examination and/or MRI and/or bone scintigraphy. Patients were excluded if they did not meet all inclusion criteria. No patients were excluded due to image quality issues. All CT examinations were conducted for clinical indications only.

In view with the follow-up data and the abovementioned reference imaging (d), the conventional CT and the spectral CT reconstructions, the target lesions and vertebrae were predefined by a senior radiologist and a fellow radiologist in consensus by documenting the position of the target lesion. They defined one single trabecular metastasis per patient. All lesions were in the range of the vertebrae T1–L5 and had been confirmed by the clinical patient report of a board-certified radiologist independent of the study.

Imaging protocol

All examinations were carried out on one clinical SDCT (IQon Spectral Detector CT, Philips Healthcare) using the build in bowtie filters of the scanner and the following scan parameters: (a) scanned slice thickness 2 mm; (b) pitch 0.671; (c) collimated detector width 64 × 0.625 mm; (d) increment along *z*-axis 1 mm; (e) rotation time 0.33 s; and (f) tube voltage 120 kV, tube current with dose modulation 80–400 mAs, average CTDIvol 11.5 mGy. The scans were reconstructed with a 512 × 512 voxel matrix. Field of view was adapted to the patient size resulting in variance of the in-plane pixel spacing. One hundred milliliters of iso-osmolar, non-ionized, iodinated contrast media (iohexol 350 mg/ml, Accupaque, GE Healthcare) were injected into an antecubital vein at 3 ml/s using an automated injector (Medrad Stellant CT infection system, Bayer Healthcare) followed by 30 ml saline flush at the same flow rate. Bolus tracking was used to start image acquisition by placing a ROI in the descending aorta and using a trigger threshold of 150 HU. The CT scans started with a delay of 50 s.

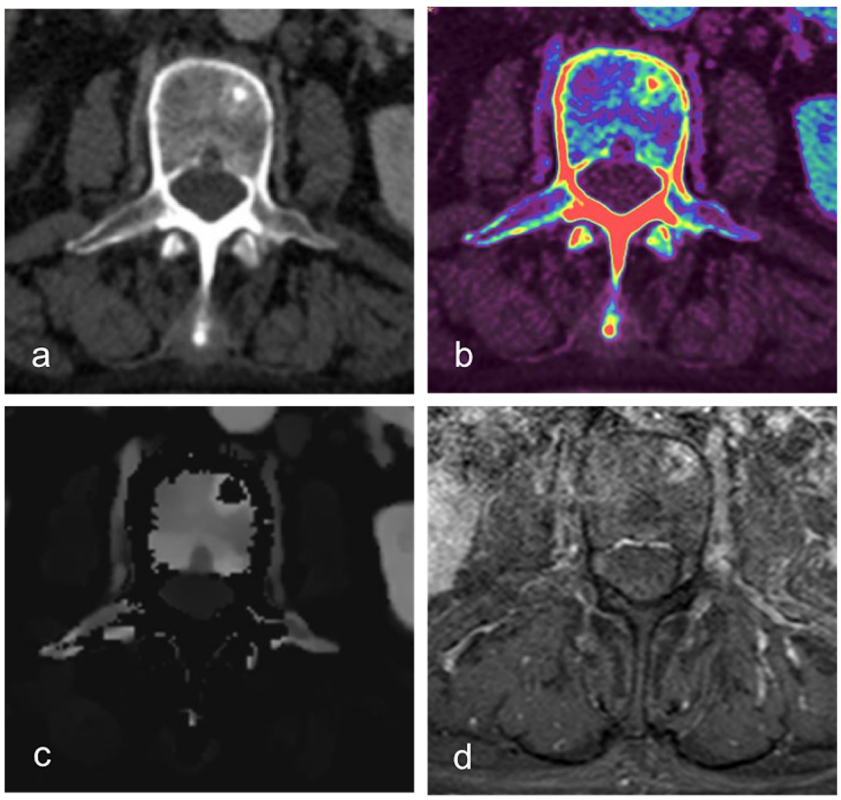

Fig. 1 Bone lesion in a 63-year-old female patient with breast cancer which was diagnosed as metastasis due to increase of size during follow-up (**a**) and MRI imaging here shown with intense contrast enhancement in T1 mDixon (**d**). Reconstructed iodine mapping from the spectral base images of SDCT exhibited an increase of iodine density adjacent to the lesion (**b**, **c**) with central artificial extinction due to calcium and iodine overlap

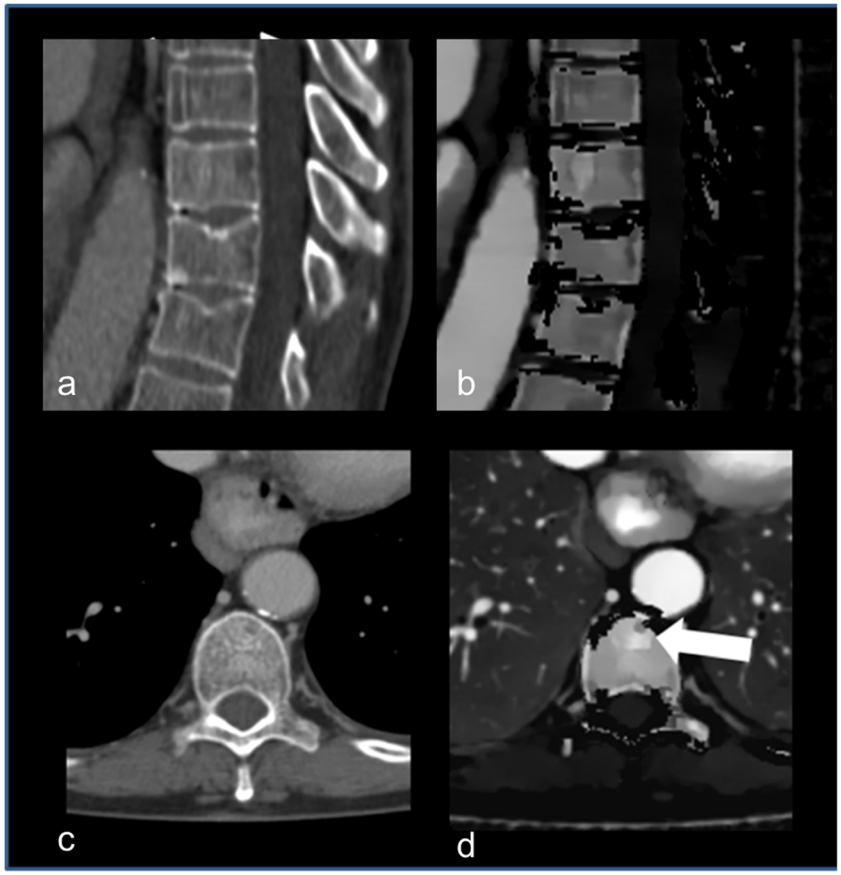

Fig. 2 Diffuse bone marrow metastasis of a thoracic vertebral body in a 66-year-old woman with NSCLC that was not detected in the radiological image analysis of the conventional CT images (**a**, **c**). MRI of the brain that was conducted to complete staging revealed suspicious signal intensities of the skull that were interpreted as diffuse bone metastases. Therefore, a post hoc analysis of the SDCT staging was conducted using iodine mapping (**b**, **d**) which showed highly suspicious bone marrow lesions with an iodine density of > 5.7 mg/ml. These proved to be metastases in bone scintigraphy and follow-up

Postprocessing and image reconstruction

Conventional image reconstructions were obtained by combination of the information from both layers. Postprocessing of the raw data included a hybrid iterative image reconstruction algorithm (iDose^4, Philips Healthcare) for conventional images. Spectral CT datasets were reconstructed using the spectral reconstruction algorithm that is provided as a standard setting (Spectral B, Philips Healthcare). Images were reconstructed in axial plane with a slice thickness of 2 mm and a section increment of 1 mm. Iodine density mapping was generated automatically, using the manufacturer software (Figs. 1 and 2, Spectral Diagnostics Suite, V8, Philips Healthcare).

Image analysis

The CT images were analyzed using the vendor-specific software (Spectral Diagnostics Suite, V8, Philips Healthcare). Two blinded radiologists with 4 years of experience in oncologic imaging conducted circular region of interest (ROI) measurements of ID within the predefined vertebral trabecular metastases of BM patients. Further, they recorded ID in normal-appearing vertebral trabecular bone of BM and NoBM patients in representative planes that were chosen by the two readers individually. ROI measurements from both readers were averaged. For further reference, both readers measured ID in the inferior vena cava, in the infrarenal aorta, and in the adjacent

Table 2 Inclusion and exclusion criteria of the study

Inclusion criteria	Exclusion criteria
Cases: all SDCT study within study period (June 2016–March 2017)	Any inclusion criteria missing
Control group: random selection of SDCT studies within study period (June 2016–March 2017)	
Diagnosis of lung cancer or breast cancer	
Prevalence of bone metastases	
Definite verification bone metastases at 6-month follow-up CT examination, MRI, and/or bone scintigraphy inferior image quality	

vertebral venous plexus after prior teaching by the senior radiologist. These reference measures were used for calculating the vertebral body reference iodine density. ROIs were adapted to the lesion, maintaining a minimum size of 0.5 cm^2.

The vBMD was determined using a CE/FDA-approved phantomless vBMD software using the conventional CT reconstructions of the SDCT scans (IntelliSpace, Philips Healthcare) and the methods described and investigated earlier [26, 27]. vBMD measurements were conducted in the lumbar vertebral bodies L1–L3. In case of fractures and/or metastases to one of these vertebrae, they were excluded from the analysis and replaced by additional measurements of T12 or L4.

Statistical analysis

Statistical analysis was performed using JMP (V12; SAS Institute) and MedCalc software (V17.7.2, MedCalc). The agreement between readers was assessed using intraclass correlation coefficient (ICC). Student's *t* test, the Wilcoxon test, and Pearson correlation coefficient were used to compare the continuous variables. The association of iodine density and metastases as well as iodine thresholds was evaluated by logistic regression analysis, followed by receiver operating characteristics (ROC). The corresponding areas under the curve (AUC) were compared non-parametrically using the DeLong method. Significant effects of possible confounding factors on the ID quantification were assessed using multivariable regression analyses, testing for residual influence. Statistical significance was defined as $p \leq 0.05$. Further results are summarized as mean ± standard deviation [28].

Results

Eighty-three patients were included: 21 with BBM, 22 with LBM, and 40 without BM (NoBM) (vertebral distribution given in appendix Fig. 1). For each BM patient, one target lesion and one reference measurement of HTB were acquired as well as one reference measurement of HTB in the BM group and the control subjects. Age of NoBM patients was slightly lower but did not differ significantly (BBM 63.9 ± 11.7 years, LBM 65.2 ± 12.7, NoBM 57.0 ± 13.7, $p = 0.07$). There was no significant difference in the distribution of gender (male/female: BBM 9m/12f, LBM 12m/10f, NoBM 15m/25f, $p = 0.53$). The vBMD was comparable between BM and NoBM patients (90.1 ± 36.8 mg/ml vs. 90.8 ± 32.5 mg/ml, $p = 0.92$).

The ICC between ID measurements of both readers was excellent (ICC 0.89). Iodine density measured in unaffected trabecular bone of NoBM and BM patients was comparable (3.8 ± 0.9 mg/ml vs. 3.5 ± 1.0, $p = 0.4$). There was a significant difference between iodine density of bone metastases compared to normal-appearing trabecular bone (5.6 ± 1.0 vs. 3.8 ± 0.9, $p < 0.0001$, Fig. 3), whereas iodine density in BBM and LBM was comparable (5.5 ± 0.8 vs. 5.6 ± 1.2, $p = 0.73$, Fig. 4). A correlation between iodine density and vBMD was found for normal-appearing bone ($r^2 = 0.39$, $p < 0.001$) but less for BM ($r^2 = 0.08$, $p = 0.06$). Further, in multivariate analysis, both age ($p = 0.0001$) and vBMD ($p = 0.02$) were independent predictors of iodine density, with a dedicated considerable influence of age on IDM (Fig. 5).

In univariate analysis, increased iodine density showed the strongest association with metastases, yielding an AUC of 0.90 with a maximum combined specificity and sensitivity of 77.5% and 90.7% when applying a threshold of 4.5 mg/ml (Fig. 6). In the same model, a slightly increased iodine density threshold of 5.0 mg/ml showed a strongly enhanced specificity of 90% with a reduction of sensitivity to 72%.

In order to improve the statistical discrimination of metastases and normal bone in addition to iodine density measures alone, we tested the following five parameters in multivariate models with ID: (a) standard deviation of mean iodine density (SD of iodine density), reference mean iodine density in (b) infrarenal aorta, (c) vena cava, and (d) vertebral venous sinus of the affected vertebra as well as (e) lumbar vBMD. In comparison to ID alone, the combined model of iodine density and the standard deviation of iodine density led to an AUC increase to 0.94 with the SD remaining significant and thus independent discriminator beyond iodine density itself ($p < 0.03$). vBMD was a significant contributor to multivariate models in combination with iodine density and SD of iodine density, increasing AUC to 0.93 and 0.95, respectively. Adjusting

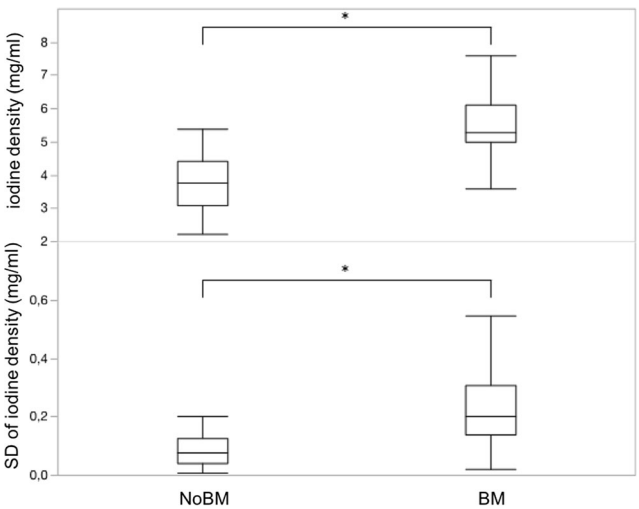

Fig. 3 Iodine density and standard deviation (SD) of iodine density are significantly higher in patients with bone metastases (BM) and patients without (NoBM, * $p < 0.0001$ each in Wilcoxon Test)

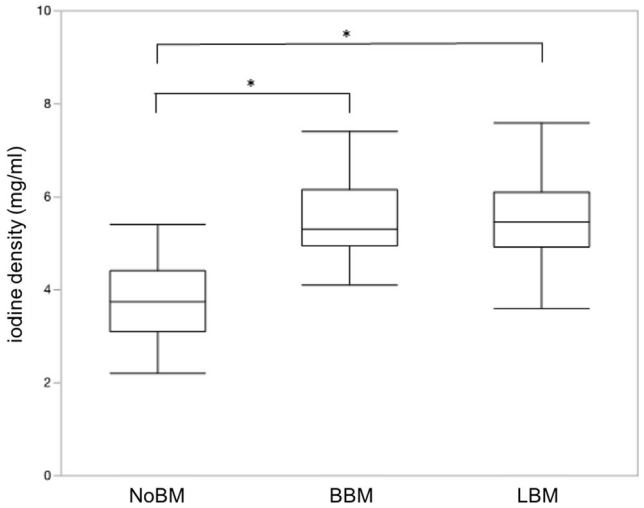

Fig. 4 Iodine density of osteolytic and osteoblastic bone metastases compared to normal-appearing trabecular bone (NoBM). BBM and LBM show a significantly higher iodine density than NoBM (*$p < 0.0001$ each in the Wilcoxon test). There is still a significant overlap between the ranges of density of BM and NoBM

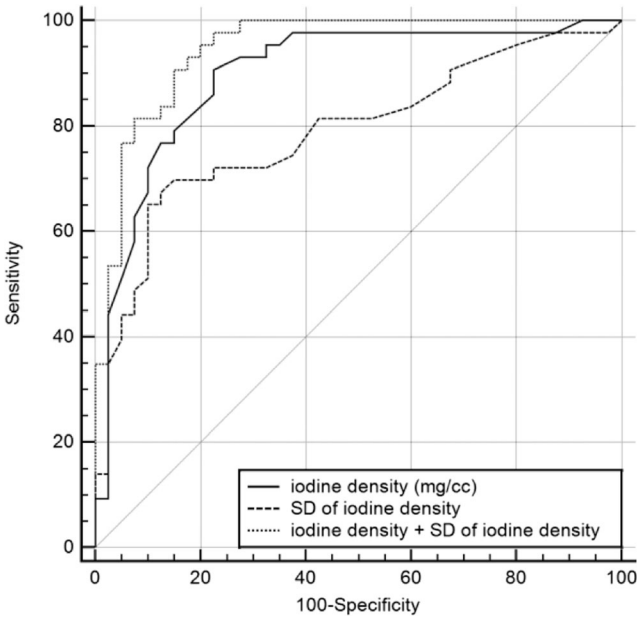

Fig. 6 ROC analysis for iodine density as discriminator between BM and normal-appearing trabecular bone (NoBM) (AUC = 0.897). Iodine density of 4.5 mg/ml yielded a specificity of 78% and a sensitivity of 91%. The iodine density threshold of 5.0 mg/ml was more specific (90%), however, less sensitive (72%). SD of iodine density (AUC = 0.79) as a measure of inhomogeneity showed an independent association with bone metastases ($p < 0.01$) in a multivariate model with iodine density (AUC = 0.95). Adjusting iodine density of BM and normal-appearing trabecular bone (NoBM) with the iodine density of the venous sinus of the same vertebra allowed full statistic discrimination of bone metastases; here, a threshold of 0.96 showed a 100% sensitivity and specificity for metastases (AUC = 1.0)

iodine density of the bone with reference iodine density in blood vessels did not yield a further improvement of AUC; however, the additional adjustment of iodine density to the density in the vertebral venous sinus (ratio of bone iodine density divided by the venous density of the same vertebra) showed a further increase of metastases discrimination (AUC = 0.98) yielding a specificity of 100% and sensitivity of 95.4% with a ratio threshold of 1.2.

Discussion

SDCT allows for reconstructions of iodine maps that enable to quantify iodine uptake in any voxel of the acquired CT scans and to perform a visual mapping of iodine distribution. In our clinical experience, ID mapping allows to detect occult bone lesions that cannot be detected with conventional CT due to the high contrast of the bone and the lack of bone destructions. As studies in regard to this mapping technique are sparse, we investigated if certain iodine density thresholds can be defined that allow for the statistical discrimination of known bone metastases from regular trabecular bone. Based on these results, the study aims to serve as proof of concept for further

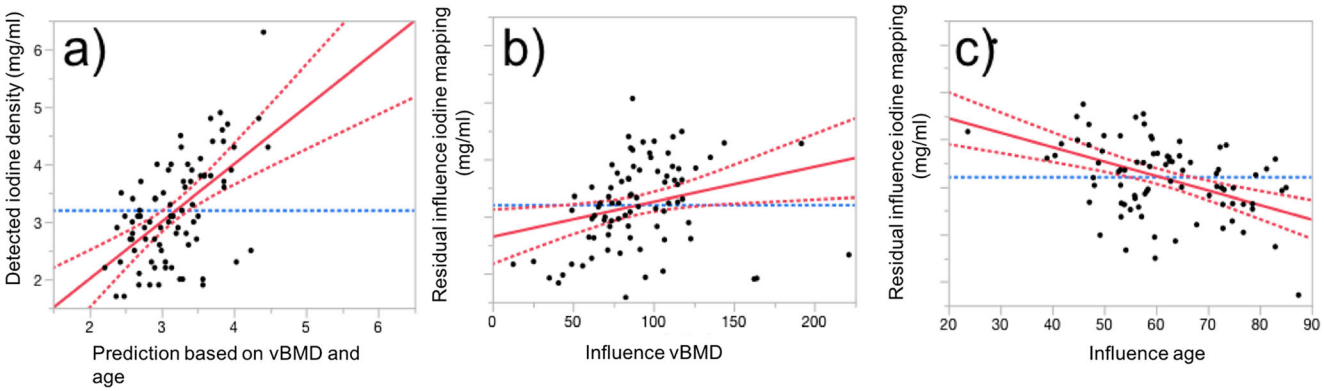

Fig. 5 Multivariate logistic regression analysis of vBMD and age as predictor of iodine density in healthy trabecular bone (**a**, $p < 0.0001$, $r^2 = 0.33$, RMSE 0.75). In the residual regression plots (**b**, **c**), both vBMD ($p < 0.05$) and age ($p < 0.0001$) are independent and significant predictors of iodine density. This implies that iodine density thresholds for the detection of metastases could be improved significantly when adjusting for vBMD and age

clinical studies and a possible future clinical application by providing preliminary reference values that might be used as an indicator for or against the differential diagnosis of vertebral metastases in SDCT as well as a systematic analysis of confounders for ID measurements in trabecular bone.

Prior studies demonstrated that dual-energy CT is useful for the detection and differentiation of malignant vertebral lesions [13, 14]. Here, especially iodine density was found to be a valuable parameter in the assessment of response to targeted therapies such as antiangiogenic treatment; however, the determination of prevalent bone metastases based on iodine density measures in comparison to soft tissue organs was found to be difficult due to (a) similar characteristics of calcium and iodine in dual-energy CT, aggravated by (b) the high intra-individual variance of bone mineral content, (c) the contrast between trabecular bone and metastases, and (d) partial volume effects of trabecular bone. Thus, it does not surprise that we found a correlation between iodine density measures and vBMD in an unaffected trabecular bone ($r^2 = 0.38$, $p < 0.0001$). This indicates that in vertebral bone, the precise material separation of calcium and iodine with dual-energy CT is hampered by higher bone mineral concentrations, especially in osteoblastic bone lesions or in younger patients. The use of increased tube voltages (140 kVp instead of 120 kVp) may improve iodine quantification due to better spectral separation and could be used in dedicated CT bone scans. However, for staging purposes, higher kVp settings should be discussed critically in view with the increased X-ray exposure and image quality in soft tissue organs [29]. Further, we found, that the iodine density in healthy trabecular bone is strongly dependent on age, independent of vBMD. This physiological observation is of particular importance; besides definition of one dedicated iodine threshold to be considered optimal, iodine density could be displayed as an adjusted T score, taking into account factors such as age and vBMD. Such improved IDM methods could also serve as a measure of viable bone marrow and as an additional CT value for the determination of fracture risk in osteoporosis, bone marrow infiltration, or depletion in hematological diseases.

For the differentiation of vertebral metastases and healthy trabecular bone in the provided setting, the acquired mean iodine density values yielded an excellent reproducibility between the readers (ICC 0.89), a high statistical sensitivity and adequate specificity to separate tumorous bone infiltrations from healthy bone marrow. In this regard, our data suggested iodine density thresholds of 4.5–5.0 mg/ml as optimal discriminator. The threshold of 4.5 mg/ml was most performant in regard to the Youden Index of ROC analysis, but did not yield optimal specificity in order to be used for confident bone lesion as there was a significant overlap of iodine density between metastatic lesions and HTB. Thus, we would recommend the far more specific threshold of 5.0 mg/ml to be tested as cut-off value in further studies.

To assess confounders of ID measurements in trabecular bone and in order to improve the statistical separation of BM, multivariate analyses were conducted, evaluating additional features to derive a more accurate statistical discrimination of metastases by the use of iodine maps. We found that adjustment of iodine density of metastases to the iodine density in the corresponding vertebral venous sinus yielded the best results. This measure reflects the healthy iodine density within the vertebra without significant bone structures deteriorating the results that adjust for the inter-individual and the observed age-related differences. Additional measures of distant vessels such as the aorta and the vena cava inferior were not effective for this purpose. Despite the high level of discriminatory power, the additional detection of vBMD and SD of iodine density was independent contributors to the multivariate models. vBMD might reflect the difficulties of accurate iodine differentiation from calcium in dual-energy CT, but it did not differ between BM and NoBM patients ($p = 0.92$). The SD of iodine density may be understood as a measure of inhomogeneity of the texture and perfusion resulting from neoangiogenesis and immature vessel structure with associated leakage [18, 19, 30].

Limiting aspects of this study are retrospective design and lack of histopathologic correlation, as the diagnosis of all the lesions was performed with regard to additional or follow-up imaging only. As the study was conducted with one SDCT scanner and a dedicated contrast medium concentration, the results cannot be applied for other scanner types and possibly do not match other contrast protocols. The results may also vary across different SDCT scanners and time-points and could be affected by reconstruction algorithms as well as size and anatomy of the lesions, which needs to be evaluated in further detail. The calculated accuracies and sensitivities should be verified in independent clinical studies since the ROIs had to be placed in a predefined area, which had to be selected based on a reference standard in retrospect. Further, there may be more confounders to iodine density measurements within the trabecular bone that should be investigated; patient weight and weight-adapted contrast medium application could have a further impact on ID quantification.

In conclusion, mean iodine density measured in spectral detector CT yields high sensitivity and adequate specificity for the statistical differentiation of vertebral trabecular metastases and healthy trabecular bone with the best overall performance using an iodine density threshold of 4.5 mg/ml. With an increased specificity of 90% and sensitivity of 72%, the threshold of 5.0 mg/ml may be of

additional value for the specific detection of trabecular bone lesions. An increased iodine density in comparison to the vertebral venous sinus, the adjustment for volumetric bone mineral density, and the standard deviation of the iodine density as a measure of inhomogeneity lead to a further improvement of lesion discrimination. Thus, iodine density quantification may provide a diagnostic value for statistical differentiation and characterization of treatment response of metastases.

Funding The authors state that this work has not received any funding.

Compliance with ethical standards

Guarantor The scientific guarantor of this publication is Jan Borggrefe.

Conflict of interest The authors of this manuscript declare relationships with the following companies: D.M. and J.B. received honorarium from Philips for scientific lectures. The authors have no conflicts of interest.

Statistics and biometry One of the authors has significant statistical expertise.

Informed consent Written informed consent was waived by the Institutional Review Board.

Ethical approval Institutional Review Board approval was obtained.

Methodology
- Retrospective
- Cross sectional study
- Performed at one institution

References

1. White AP, Kwon BK, Lindskog DM, Friedlaender GE, Grauer JN (2006) Metastatic disease of the spine. J Am Acad Orthop Surg 14: 587–598
2. Guillevin R, Vallee JN, Lafitte F, Menuel C, Duverneuil NM, Chiras J (2007) Spine metastasis imaging: review of the literature. J Neuroradiol 34:311–321
3. Roodman GD (2004) Mechanisms of bone metastasis. N Engl J Med 350:1655–1664. https://doi.org/10.1056/NEJMra030831
4. Reddi AH, Roodman D, Freeman C, Mohla S (2003) Mechanisms of tumor metastasis to the bone: challenges and opportunities. J Bone Miner Res 18:190–194. https://doi.org/10.1359/jbmr.2003.18.2.190
5. Toth DF, Töpker M, Mayerhöfer ME et al (2013) Rapid detection of bone metastasis at thoracoabdominal CT: accuracy and efficiency of a new visualization algorithm. Radiology 270:130789. https://doi.org/10.1148/radiol.13130789
6. Horger M, Thaiss WM, Wiesinger B et al (2017) Longitudinal computed tomography monitoring of pelvic bones in patients with breast cancer using automated bone subtraction software. Invest Radiol 52: 288–294. https://doi.org/10.1097/RLI.0000000000000343
7. Mundy GR (2002) Metastasis to bone: causes, consequences and therapeutic opportunities. Nat Rev Cancer 2:584–593. https://doi.org/10.1038/nrc867
8. Rybak LD, Rosenthal DI (2001) Radiological imaging for the diagnosis of bone metastases. Q J Nucl Med 45:53–64
9. Heindel W, Gübitz R, Vieth V, Weckesser M, Schober O, Schäfers M (2014) The diagnostic imaging of bone metastases. Dtsch Arztebl Int 111:741–747. https://doi.org/10.3238/arztebl.2014.0741
10. Silva AC, Morse BG, Hara AK, Paden RG, Hongo N, Pavlicek W (2011) Dual-energy (spectral) CT: applications in abdominal imaging. Radiographics 31:1031–1046. https://doi.org/10.1148/rg.314105159
11. McCollough CH, Leng S, Yu L, Fletcher JG (2015) Dual- and multi-energy CT: principles, technical approaches, and clinical applications. Radiology 276:637–653. https://doi.org/10.1148/radiol.2015142631
12. He P, Wei B, Cong W, Wang G (2012) Optimization of K-edge imaging with spectral CT. Med Phys 39:6572–6579. https://doi.org/10.1118/1.4754587
13. Zheng S, Dong Y, Miao Y et al (2014) Differentiation of osteolytic metastases and Schmorl's nodes in cancer patients using dual-energy CT: advantage of spectral CT imaging. Eur J Radiol 83: 1216–1221. https://doi.org/10.1016/j.ejrad.2014.02.003
14. Dong Y, Zheng S, Machida H et al (2015) Differential diagnosis of osteoblastic metastases from bone islands in patients with lung cancer by single-source dual-energy CT: advantages of spectral CT imaging. Eur J Radiol 84:901–907. https://doi.org/10.1016/j.ejrad.2015.01.007
15. Neuhaus V, Abdullayev N, Große Hokamp N et al (2017) Improvement of image quality in unenhanced dual-layer CT of the head using virtual monoenergetic images compared. Invest Radiol 52:470–476. https://doi.org/10.1097/RLI.0000000000000367
16. Neuhaus V, Große Hokamp N, Abdullayev N et al (2017) Metal artifact reduction by dual-layer computed tomography using virtual monoenergetic images. Eur J Radiol 93. https://doi.org/10.1016/j.ejrad.2017.05.013
17. Borggrefe J, Kottlors J, Mirza M et al (2017) Differentiation of clot composition using conventional and dual-energy computed tomography. Clin Neuroradiol. https://doi.org/10.1007/s00062-017-0599-3
18. Hanahan D, Weinberg RA (2011) Hallmarks of cancer: the next generation. Cell 144:646–674
19. Joyce JA, Pollard JW (2009) Microenvironmental regulation of metastasis. Nat Rev Cancer 9:239–252. https://doi.org/10.1038/nrc2618
20. Dvorak HF, Detmar M, Claffey KP, Nagy JA, van de Water L, Senger DR (1995) Vascular permeability factor/ vascular endothelial growth factor: an important mediator of angiogenesis in malignancy and inflammation. Int Arch Allergy Immunol 107:233–235. https://doi.org/10.1159/000236988
21. Vaupel P, Kallinowski F, Okunieff P (1989) Blood flow, oxygen and nutrient supply, and metabolic microenvironment of human tumors: a review. Cancer Res 49:6449–6465
22. Lee TY, Purdie TG, Stewart E (2003) CT imaging of angiogenesis. Q J Nucl Med 47:171–187. https://doi.org/10.1016/j.cpet.2009.04.011
23. Axel L (1980) Cerebral blood flow determination by rapid-sequence computed tomography: theoretical analysis. Radiology 137:679–686. https://doi.org/10.1148/radiology.137.3.7003648
24. Miles KA (1991) Measurement of tissue perfusion by dynamic computed tomography. Br J Radiol 64:409–412. https://doi.org/10.1259/0007-1285-64-761-409
25. Eisenhauer EA, Therasse P, Bogaerts J et al (2009) New response evaluation criteria in solid tumours: revised RECIST guideline (version 1.1). Eur J Cancer 45:228–247. https://doi.org/10.1016/j.ejca.2008.10.026

26. Neuhaus V, Abdullayev N, Hellmich M et al (2016) Association of quality and QUANTITY of bone metastases and computed tomography volumetric bone mineral density with prevalence of vertebral fractures in breast cancer patients. Clin Breast Cancer. https://doi.org/10.1016/j.clbc.2016.05.010
27. Mueller DK, Kutscherenko A, Bartel H, Vlassenbroek A, Ourednicek P, Erckenbrecht J (2011) Phantom-less QCT BMD system as screening tool for osteoporosis without additional radiation. Eur J Radiol 79:375–381. https://doi.org/10.1016/j.ejrad.2010.02.008
28. DeLong ER, DeLong DM, Clarke-Pearson DL (1988) Comparing the areas under two or more correlated receiver operating characteristic curves: a nonparametric approach. Biometrics 44:837. https://doi.org/10.2307/2531595
29. Pelgrim GJ, van Hamersvelt RW, Willemink MJ et al (2017) Accuracy of iodine quantification using dual energy CT in latest generation dual source and dual layer CT. Eur Radiol 27:3904–3912. https://doi.org/10.1007/s00330-017-4752-9
30. Folkman J (1990) What is the evidence that tumors are angiogenesis dependent? J Natl Cancer Inst 82:4–7